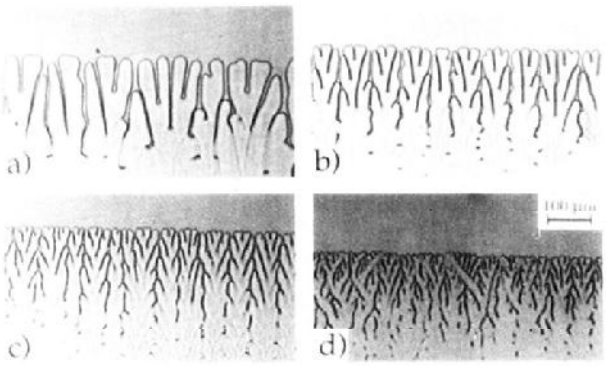

FIG. 10. Seaweed morphology in a crystal close to the {111} orientation. (a) $V=8.6\ \mu m\,s^{-1}$ ($\approx 4.5 V_{CS}$); (b) $V=29\ \mu m\,s^{-1}$ ($\approx 15 V_{CS}$); (c) $V=64\ \mu m\,s^{-1}$ ($\approx 34 V_{CS}$); (d) $V=100\ \mu m\,s^{-1}$ ($\approx 53 V_{CS}$).

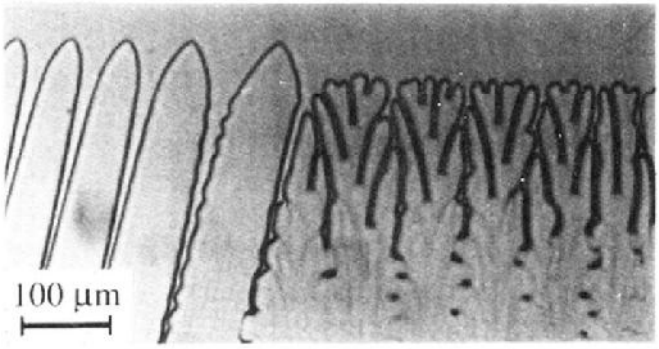

FIG. 11. Grain boundary between a tilted-dendritic grain and a seaweed grain. $V=29\ \mu m\ s^{-1}$ ($\approx 15 V_{CS}$).

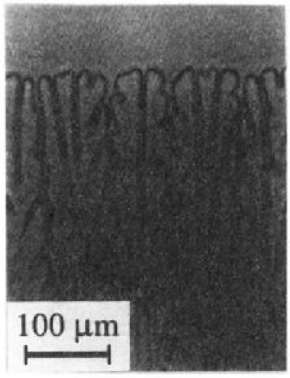

FIG. 15. A seaweed cell containing one doublon whose lifetime was about 30 s ($\approx 60\tau_d$). $V = 32\ \mu m\ s^{-1}$ ($\approx 17 V_{CS}$).

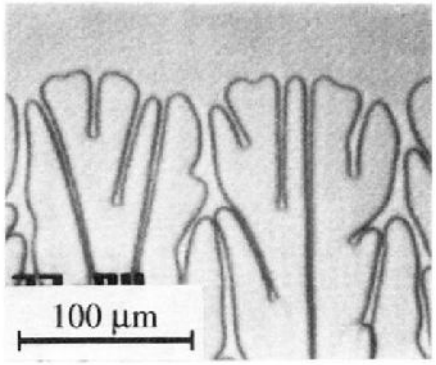

FIG. 17. Enlarged view of a seaweed pattern. $V=32\ \mu m\,s^{-1}$ ($\approx 17 V_{CS}$). Note, from left to right, a doublon joining a wide groove, a newly created doublon, and a triplet structure.

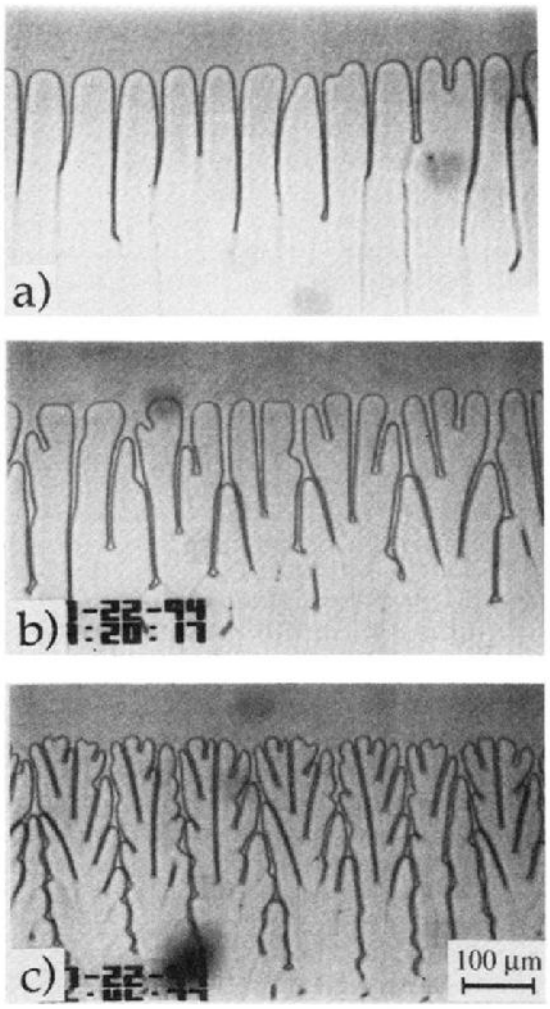

FIG. 18. The low-velocity transition in a nearly {111}-oriented grain. (a) $V=4\ \mu m\ s^{-1}$ ($\approx 2.1 V_{CS}$). (b) 8.5 $\mu m\, s^{-1}$ ($\approx 4.5 V_{CS}$); (c) 32 $\mu m\, s^{-1}$ ($\approx 17 V_{CS}$).

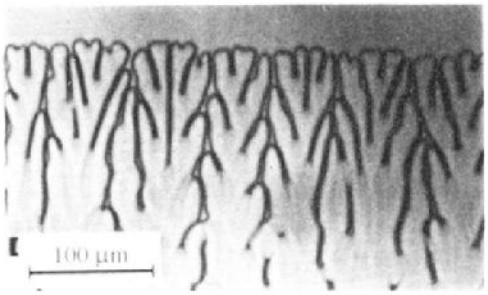

FIG. 2. Seaweed pattern in a nearly {111}-oriented crystal. The growth direction is upward, as for all the photographs in this article. The pulling velocity $V = 64\ \mu\text{m s}^{-1} (\approx 33.7 V_{\text{CS}})$.

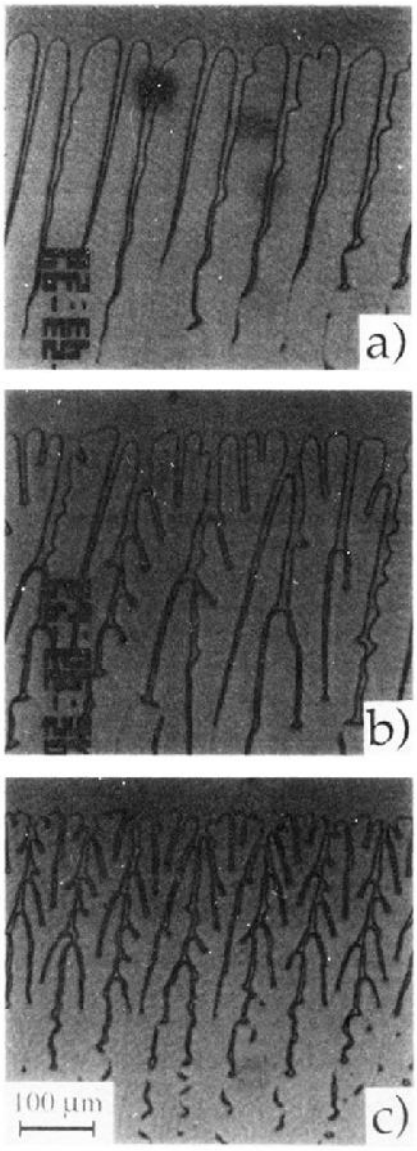

FIG. 21. Tilted-seaweed morphology in a crystal close to (but not exactly in) the (111) orientation. (a) $V=12.5$ $\mu m\,s^{-1}$ ($\approx 6.5 V_{CS}$); (b) $V=19.6$ $\mu m\,s^{-1}$ ($\approx 10.3 V_{CS}$); (c) $V=32$ $\mu m\,s^{-1}$ ($\approx 16.8 V_{CS}$).

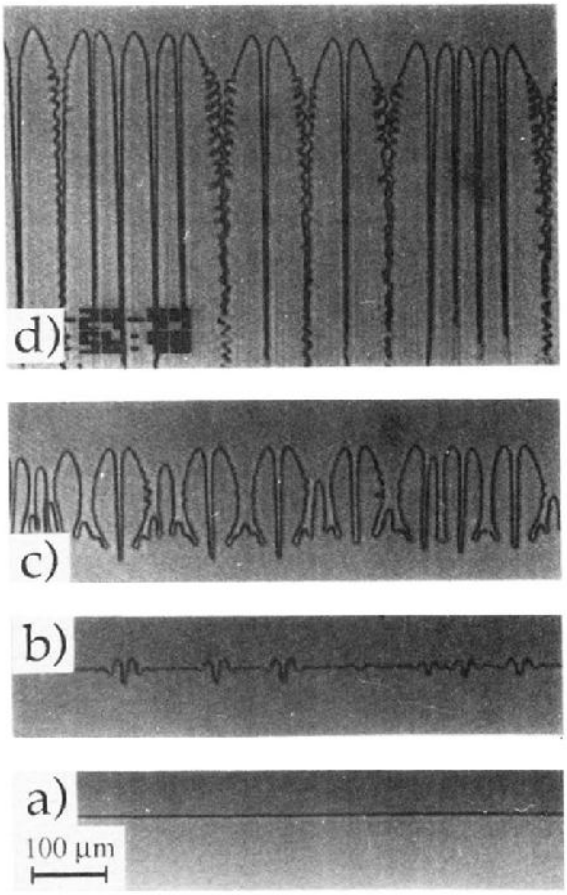

FIG. 22. Crystal close to the (001)[100] orientation. Initial transient of the first run at $V=103\ \mu m\,s^{-1}$ ($V\approx 54V_{CS}$; $l_d=4.9\ \mu m$; $\tau_d=0.05$ s). (a) $t=0$ s (onset of the pulling); (b) $t=6.4$ s; (c) $t=8.1$ s; (d) $t=42$ s. Note the dendritic doublons in the middle and the multiplet on the right. The tilt angle of the dendrites is about 2°, with a negligible dispersion.

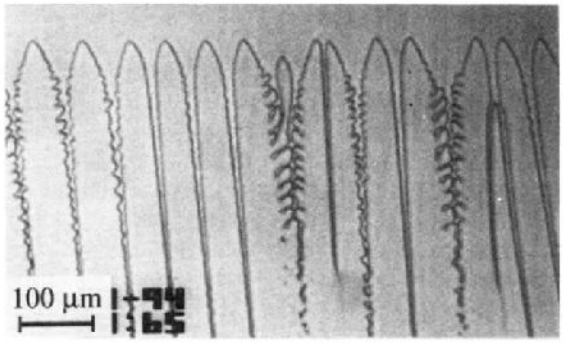

FIG. 23. Same grain as in Fig. 22. Second run at $V=103$ $\mu m\,s^{-1}$. The tilt angle of the dendrites is $5°\pm2°$. This figure corresponds to $t=90$ s in the ST diagram shown in Fig. 24. Note the source operating by a tail-instability mechanism next to the doublon.

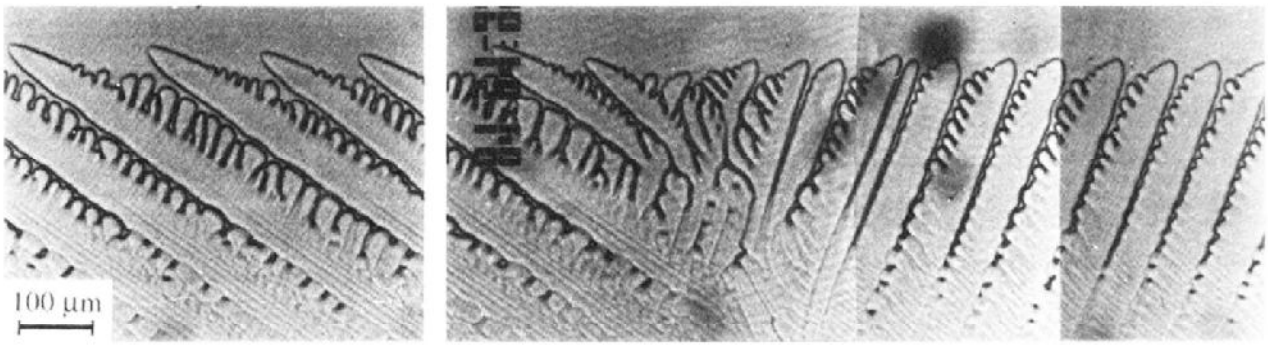

FIG. 25. Competition between two tilted dendritic states in a crystal close to the degenerate orientation (same crystal as in Fig. 4). $V = 32\ \mu\text{m s}^{-1}$ ($\approx 17 V_{CS}$). Note the dynamic wall between two domains occupied by the [100] ($\phi \approx 22°$ to the right) and the [010] dendritic states ($\phi \approx 54°$ to the left), respectively.

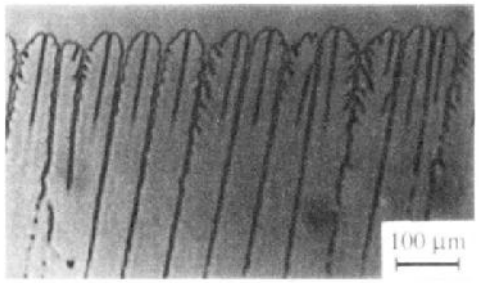

FIG. 3. Doublons in a nearly {001}⟨100⟩-oriented crystal. $V = 103\ \mu m\ s^{-1} \approx 27 V_{CS}$ ($C_\infty \approx 4\%$ in this experiment).

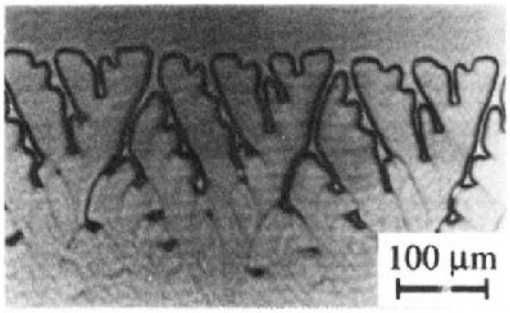

FIG. 4. Degenerate pattern in a nearly {001}⟨110⟩-oriented grain. $V=7\ \mu\text{m s}^{-1}$ ($\approx 3.7 V_{CS}$).

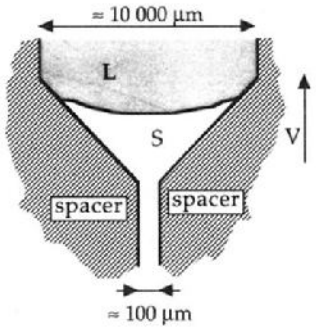

FIG. 6. Sketch of the method of obtaining single crystals (L, liquid; S, solid).

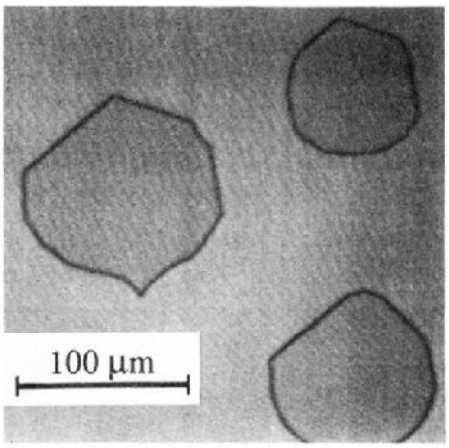

FIG. 7. Partly faceted residual-gas inclusions in a nearly {111}-oriented crystal. Note that the orientation of the facets is the same in all the inclusions.

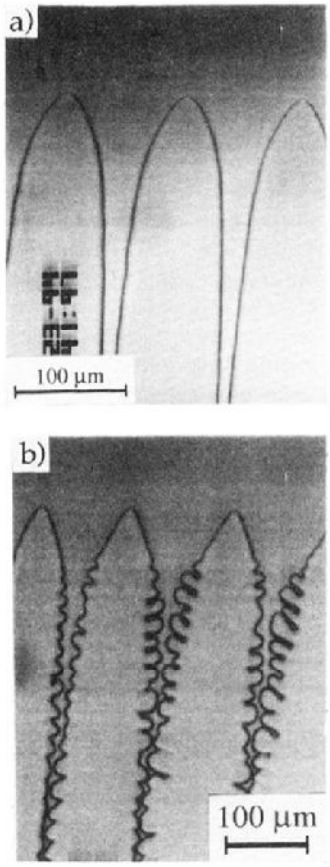

FIG. 8. Dendrite tips in a nearly {001}⟨100⟩-oriented crystal (see Table III). (a) $V=13\ \mu m\ s^{-1}$; (b) $V=35\ \mu m\ s^{-1}$.

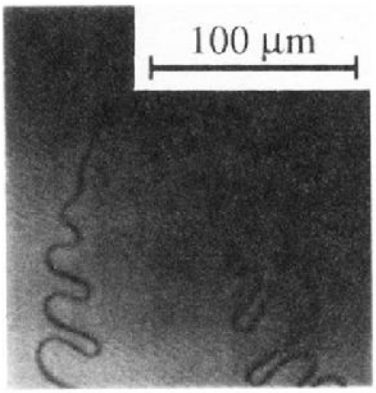

FIG. 9. Dendrite tip in a crystal relatively close to a {111} orientation (off-plane misorientation angle $\approx 7°$). $V = 14$ $\mu m\, s^{-1}$.